IEEE Access
Multidisciplinary | Rapid Review | Open Access Journal

Received August 13, 2020, accepted September 28, 2020, date of publication October 14, 2020, date of current version October 26, 2020.

Digital Object Identifier 10.1109/ACCESS.2020.3030953

Using Biomimetic Scaffold Platform to Detect Growth Factor Induced Changes in Migration Dynamics of Nasopharyngeal Epithelial Cells

BOWIE P. LAM[1,2], YUN WAH LAM[2,3], AND STELLA W. PANG[1,2], (Fellow, IEEE)

[1]Department of Electrical Engineering, City University of Hong Kong, Hong Kong
[2]Centre for Biosystems, Neuroscience, and Nanotechnology, City University of Hong Kong, Hong Kong
[3]Department of Chemistry, City University of Hong Kong, Hong Kong

Corresponding author: Stella W. Pang (pang@cityu.edu.hk)

This work was supported in part by the Centre for Biosystems, Neuroscience, and Nanotechnology, City University of Hong Kong, under Grant 9360148 and Grant 9380062; and in part by the University Grants Council of Hong Kong (GRF and CRF Projects) under Grant 11247716, Grant 11218017, Grant 11213018, Grant 11212519, and Grant C1013-15G.

ABSTRACT A polydimethylsiloxane two-layer scaffold platform was designed to provide a three-dimensional biomimetic microsystem that allows the detection of epithelial-to-mesenchymal transition without the use of specific biomarkers. As a proof of concept, a novel microsystem that consisted of two layers of 15 μm thick grating structures was developed. These layers had gratings with 40 μm wide ridges and 10 μm wide trenches, and they were stacked together to form a scaffold platform. To investigate the feasibility of using the engineered platforms for detecting changes in epithelial-to-mesenchymal transition, transforming growth factor beta-1 was added to an untransformed nasopharyngeal epithelial cell line. On flat polydimethylsiloxane surfaces, transforming growth factor beta-1 did not significantly affect nasopharyngeal epithelial size, migration speed, or directionality. However, the effect of transforming growth factor beta-1 treatment on migration speed of nasopharyngeal epithelial cells cultured on the two-layer scaffold platform was significantly different. Furthermore, while almost no untreated nasopharyngeal epithelial cells could squeeze into the 10 μm wide trenches, 21% of the transforming growth factor beta-1 treated nasopharyngeal epithelial cells exhibited traversing behaviors on the two-layer scaffold platforms. Moreover, fibronectin coating on the trenches and bottom layers of the scaffold platforms further enhanced the transforming growth factor beta-1-induced traversing of nasopharyngeal epithelial cells into the narrow trenches. These results demonstrate that the engineered two-layer scaffold microsystem can be used to monitor epithelial-to-mesenchymal transition induced changes in cell migration and invasiveness, paving the way of using these platforms in high throughput drug screening.

INDEX TERMS 3D scaffold platform, cell migration, epithelial-to-mesenchymal transition, nasopharyngeal cell, traversing into narrow trenches.

I. INTRODUCTION

In vitro studies are an essential stage in the drug discovery process [1], in which the combination of cell culture and high-throughput screening (HTS) technologies, with robotics workstation and automated data analysis, allow the rapid screening of chemical libraries for bioactivities [2]. Despite its power, *in vitro* results are often associated with high false identification rates, which puts pressure on the subsequent validation by the use of animal models, which results in drawbacks such as restricted testing procedures, availability of subjects, and ethical concerns [3], [4]. It is therefore imperative to improve the accuracy of *in vitro* testing by enhancing the physiological relevance of the screening platform.

Traditionally, primary test of soluble factors involves simple viability testing of cell culture. Most of these platforms consist of two-dimensional (2D) cell culture models. However, three-dimensional (3D) structures can better resemble a biomimetic microenvironment, which is critical in *in vitro* experiment since it often affects the cellular responses to the testing conditions [3]. Biomimetic structures have also been designed using different materials such as collagen, gelatin,

The associate editor coordinating the review of this manuscript and approving it for publication was Victor Hugo Albuquerque.

and fibrin for *in vitro* experiment [5], [6]. To automate the process and to reduce the complicated procedures for controlling the environmental condition for testing, microfluidic devices have been used [2], [7], [8]. For example, microfluidic platforms have been designed to automatically generate serial dilutions of each tested compound, reducing the time and error associated with pipetting [2].

Apart from cytotoxicity tests, recent developments in automated high-content imaging systems have allowed the measurement of growth kinetics, biomarker expression, and morphometric parameters indicative of specific molecular pathways [9], [10]. Of these pathways, cell invasiveness is one of the most important hallmarks of metastatic cancer cells. However, it is difficult to observe cell invasion and viability simultaneously with currently available screening methods [6]. The biomimetic structures built using natural materials to work as a filter can detect cell invasiveness. Using this model, designed 3D hydrogels can provide the chemical and physical environment for testing compound effectivity by observing the cell invasiveness and viability with the help of fluorescent staining and 3D imaging [6]. However, most of these platforms are complicated to construct and tedious to use for HTS. Furthermore, the diffusion kinetics of tested compounds in the hydrogel cannot be controlled precisely, leading to difficulties in data interpretation. Alternatively, cell invasiveness can be inferred from changes in cytoskeletal organization and expression of biomarkers. However, the detection of these parameters requires expensive reagents, tedious procedures and sophisticated imaging equipment that are often incompatible with high throughput workflows.

Migration behaviors of cultured cells on 2D platforms with different engineered topographies have been studied extensively [11]. We and others have demonstrated that cell culturing environment can be fabricated with different topographies [12]. Engineered platforms with confined microchannels have been fabricated using polyacrylamide hydrogel with extracellular matrix (ECM) proteins conjugated to control the stiffness and provide biochemical ligands for cell adhesion. The hydrogel was polymerized and demolded from a stamp to create microchannels with different widths for the investigation [13]. Although the hydrogel platforms have provided 3D ECMs, cells migrated in 2D manner in the microchannels. Another study also used microfluidic channels to investigate the cell migration behaviours driven by water permeation [14]. Microfluidic devices allow *in vitro* experiments with controllable physical and biochemical environment for better understanding of the underlying mechanisms of cell migration, which can be applied to HTS [15]. However, all these studies focused on the lateral movement of cells on different physical confinements.

In particular, we have recently shown that the metastatic status of cancer cells could be manifested in the cell migration behaviors on 2D grating structures [12]. These behaviors, including changes in migration speed and directionality, are readily and quickly detectable by low magnification bright-field (BF) microscopy. These microsystems thus provide an alternative approach of assessing cell invasiveness in lieu of any gel matrix, thus potentially simplifying the platform construction and allowing a more precise control of chemical concentrations in the test. As a proof of concept, the present study aimed to investigate the feasibility of detecting the local epithelial-to-mesenchymal transition (EMT) induced by the environmental conditions on the migration kinetics of cultured cells through the use of an engineered platform.

In Southern China and Southeast Asia, nasopharyngeal carcinoma (NPC) is one of the most common and highly invasive carcinomas [16]–[18]. It has been reported that transforming growth factor beta-1 (TGF-β1) upregulates the formation of invadosomes of nasopharyngeal cells which are responsible for cell invasion and metastasis while the serum of NPC patients normally have higher TGF-β1 level [18]. TGF-β1 is an inflammatory cytokine, which is present in many biological activities. It can suppress the tumor progression in early stage, but it also promotes tumor progression [19], [20]. In addition, the treatment of untransformed nasopharyngeal epithelial cells, such as the NP460 cell line [18], with TGF-β1 is known to trigger invadosome formation and EMT, an important process for tumor progression, usually associated with the loss of cell-cell adhesion, changes in cell-matrix interaction, and enhancement of cell migration and invasion [21], [22]. In this project, the migration and traversing behaviors of NP460 cells, with the cell size of 15-20 μm, on engineered double-layer scaffold platforms were studied. The migration trajectories, by BF microscopy, of NP460 cells undergoing TGF-β1-induced EMT under different surface conditions were monitored.

Polydimethylsiloxane (PDMS)-based scaffold was designed with interconnected macropores for hepatocytes cells *in vitro* experiments to assess the cell responses to drug. Although the system provided a physiological relevant model for screening, the cell morphology changes and responses could only be observed after immunofluorescence staining or with additional hepatocyte functional assay. Another PDMS scaffold with micropillars was used to mimic the microenvironment of brain for testing of drug related to brain injury through the investigation on the changes in protein expressions and glutamate release level, which cannot be assessed using simple optical microscopy. All these PDMS scaffolds provided a useful model for *in vitro* drug screening but the detection methods remained complicated and cannot be adapted to automation. In this project, as the NP460 cell migration was monitored by tracking the traversing behaviors of NP460 cells into the narrow trenches on the engineered platforms. The effectiveness of treatment can be evaluated using BF microscopy without the complicated and expensive immunofluorescence staining and confocal imaging. Software with machine learning can be used to identify subsets of macrophage from their size and morphology and for motion tracking of single cells. The captured time-lapse movies of cells on the scaffold platforms can be analyzed automatically using similar tools to increase the throughput. Other than detection of changes in EMT of cells induced

by environmental conditions, the proposed scaffold platforms can also be used for low cost and high throughout drug screening.

II. RESULTS AND DISCUSSION

A. DOUBLE-LAYER SCAFFOLD PLATFORM AS CELL CULTURE SUBSTRATE

Many microsystems were designed to provide a biomimetic environment for *in vitro* studies [7], [23]–[28]. However, most designed platforms were not fully controlled with desired dimensions. Moreover, the procedures of detecting EMT changes in cells are complicated and time-consuming. The aim of this project was to design a 3D cell culture platform that allows the rapid detection of changes in cell invasiveness induced by exogenous molecules through simple BF microscopy. A scaffold platform consisted of double layers of grating structures were fabricated as shown in Fig. 1 using the imprint technology. Detail description of the fabrication technology as shown in Fig. 1 (a-b) for the two-layer scaffold platforms will be revealed in the later section 3.1. Figures 1 (c-d) show the design of the two-layer scaffold platforms with 40 μm wide ridges, 10 μm wide trenches, and 15 μm deep grating structures for each layer. The two layers of grating structures were aligned with 90° offset between their grating orientation. The scanning electron micrographs (SEM) in Figs. 1 (c-d) show the fabricated PDMS platforms had smooth surfaces and vertical trench sidewalls of both layers for NP460 cell attachment. The trench depth was close to the average human cell size [29], [30], and the width of the ridges and trenches were designed to be much larger and much narrower than the typical size of individual NP460 cells (15 - 20 μm in diameter), respectively. From our previous study, invasive nasopharyngeal carcinoma (NPC43, 15 - 20 μm in diameter) and NP460 cells were seeded on single layer of 15 μm deep grating platforms with 40 μm ridges and 10 μm trenches, but none of them were found in the 10 μm wide trenches. However, for the designed scaffold platforms used in this study, a number of cancerous NPC43 cells were able to squeeze into 10 μm wide trenches while epithelial NP460 cells were observed to predominately stayed on top of the 40 μm wide ridges, possibly because the ridges were much wider than the size of NP460 cells. Considering NP460 cells studied in this project were normal epithelial cells that were less invasive than carcinoma cells, thus less likely to traverse to the narrow trenches. Since the 10 μm wide trenches are narrower than the average cell size, NP460 cells typically cannot squeeze into these narrow trenches. Rather, NP460 cells would attach onto the 40 μm wide ridges of the top layer once seeded onto the platforms.

B. REDISTRIBUTION AND UPREGULATION OF VIMENTIN AND β- CATENIN IN TGF-β1-TREATED NP460 CELLS

After incubating the NP460 cells overnight and then treating them with 5 ng/ml TGF-β1 for 24 h on a flat glass surface at 37 °C with 5% CO_2 supply, the expression of vimentin and

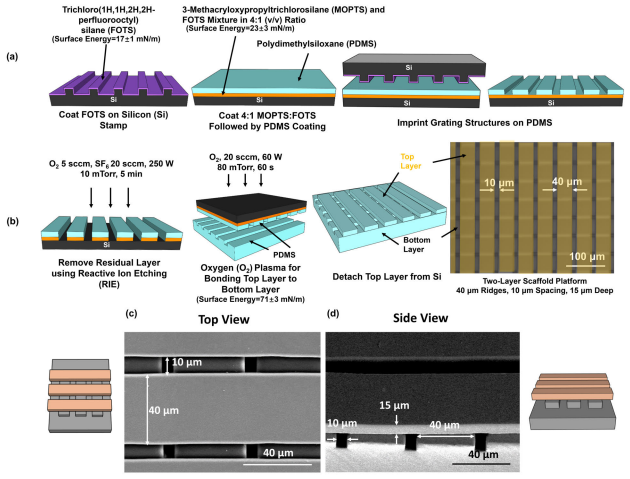

FIGURE 1. Fabrication technology of two-layer scaffold platforms. (a) Si stamp was coated with FOTS while flat Si substrate was coated with MOPTS and FOTS mixture, followed by PDMS coating. Patterns from Si stamp were transferred to PDMS by imprint. (b) Removed PDMS residual layer after imprint. Top and bottom layers were treated with O_2 plasma for bonding. SEM of two-layer scaffold platform from (c) top view and (d) side view. Both top and bottom layers were 15 μm thick gratings with 40 μm ridges and 10 μm trenches.

β-catenin from NP460 cells were investigated. Both vimentin and β-catenin are usually regarded as biomarkers of EMT. Vimentin functions as a component of cytoskeleton and is expressed in a well-regulated fashion while vimentin expression is related to cell invasiveness in terms of migration and adhesion [31]. Earlier work has demonstrated that vimentin promotes cell migration by interacting with actin, focal adhesions, and microtubules, which are important intracellular structures for cell movement. Higher level of vimentin expression was usually found in invasive cells with high motility [32]. β-catenin is involved in cell-cell adhesion while some reported that the transformation of normal cells to malignant cells was triggered by unusual expression of β-catenin [33], [34]. Previous study also shows that upregulation of β-catenin promotes the migration and invasiveness of renal cells using *in vitro* transwell assay [35]. Figure 2 shows the fluorescent staining of nuclei, actin, vimentin, and β-catenin of NP460 cells with and without the 5 ng/ml TGF-β1 treatment for 24 h on a flat glass surface. The nuclei of NP460 cells were counterstained with H33342 and shown in blue color while the transfected LifeAct of NP460 cells representing the actin of the cells were labeled in red color. The stained vimentin and β-catenin, EMT biomarkers of NP460 cells, were shown in green color and they were separately merged with the fluorescent images of the cell nuclei and actin for observation. Although only a slight increase in vimentin expression was observed after the addition of TGF-β1, NP460 cells treated by TGF-β1 demonstrated significant increase in β-catenin expression as shown in Fig. 2 (c). Furthermore, when compared to the untreated NP460 cells, discontinuous vimentin filament intercrossed with each other and formed a larger network-like structure in NP460 cells after TGF-β1 addition. The results show that

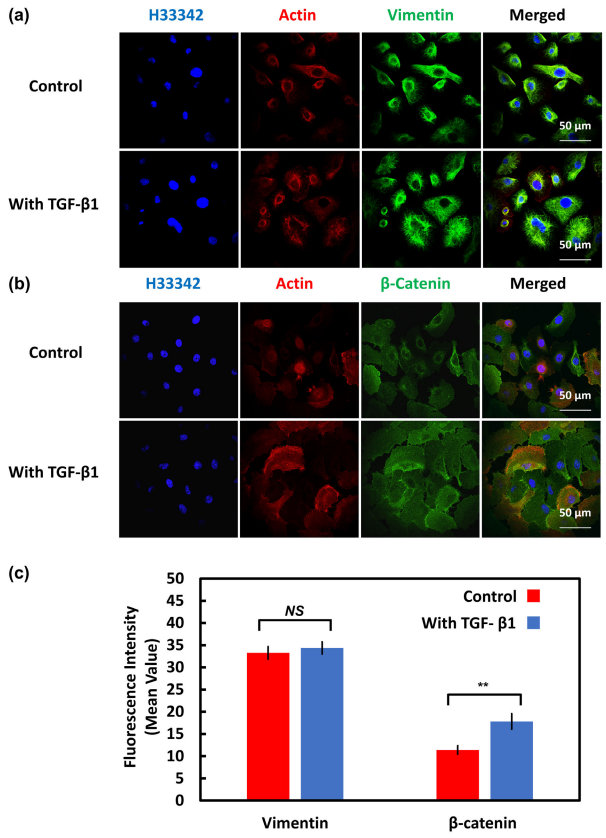

FIGURE 2. Immunofluorescence staining of (a) vimentin and (b) β-Catenin of NP460 cells with and without TGF-β1. (c) Fluorescence intensity of vimentin and β-catenin staining on NP460 cells with and without TGF-β1 (one-way ANOVA test, *NS* – Not Significant, **p<0.01).

5 ng/ml TGF-β1 could induce the EMT markers, vimentin and β-catenin, in NP460 cells.

1) MIGRATION SPEED AND DIRECTIONALITY OF NP460 CELLS ON SCAFFOLD PLATFORMS

The footprint area of NP460 cells with and without TGF-β1 stimulation on flat PDMS platforms was measured over an imaging time of 15 h as shown in Supplementary Fig. S1. The individual cell size fluctuated during 15 h of migration. The NP460 cells moved randomly instead of just staying still and spreading on the PDMS platforms to reach the plateau of their cell size. Cell movement depends on the adhesion and detachment from the surface. The cell area decreased when the cell trailing edge detached from the platform and the cell body contracted. Although the final projected area of cells could not be obtained as the cell movement was not synchronized, the result showed that there was no significant difference on the NP460 cell size even at different time point during the 15 h of imaging with and without TGF-β1 treatment. The migration trajectories shown in Fig. 3 (a) demonstrate movement of NP460 cells with and without TGF-β1 activation on flat and two-layer scaffold platforms over the 15 h imaging period. Figure 3 (b) shows the cell migration speed separately in Vx and Vy directions which are parallel to the grating orientation of the bottom and top layers, respectively. The deviation angle represents the cell migration directionality on platforms, and 45° means the cells moved randomly without orientation preference. On flat PDMS, the treated NP460 cells moved at similar speed as the NP460 cells without TGF-β1 treatment, and both NP460 cells with and without TGF-β1 activation migrated randomly with 47° deviation angle measured from x-axis. Taken together, these data indicate that it is impossible to detect the effects of TGF-β1 on NP460 cells merely from cell morphology, size, or migration dynamics without using biomarkers.

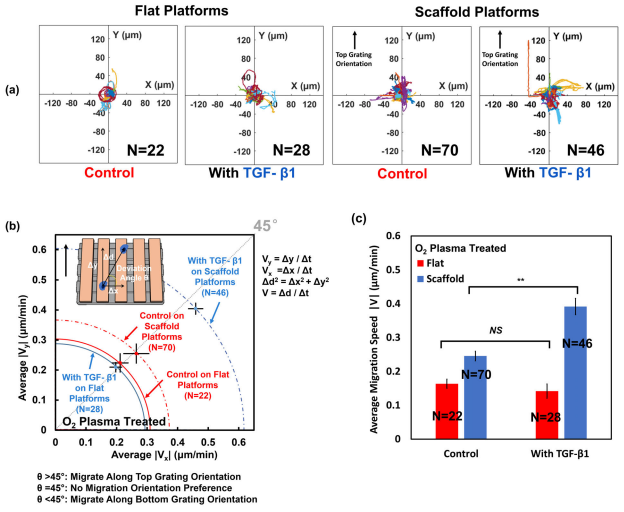

FIGURE 3. (a) Trajectories of NP460 cells on flat and two-layer scaffold platforms. (b) NP460 cell migration speed and orientation preference. (c) Migration speed of NP460 cells on O_2 plasma treated flat and two-layer scaffold platforms with and without TGF-β1 (one-way ANOVA test, *NS* – Not Significant, **p<0.01).

The effect of TGF-β1 on NP460 cells was then observed on the two-layer scaffold platform. Although the designed two-layer scaffold platforms did not provide differential migration guidance for NP460 cells with and without TGF-β1 activation (41° and 44° deviation angle from x-axis, respectively) as shown in Fig. 3 (b). Figures 3 (b-c) show TGF-β1 treated NP460 cells moved faster than the untreated ones by 60% on the scaffold platforms (0.39 μm/min compared to 0.25 μm/min for the untreated cells, **p<0.01, one-way analysis of variance (ANOVA)). Hence, NP460 cells with and without TGF-β1 treatment responded differently in the 3D microenvironment. These results are consistent with our previous work that demonstrated different migration behaviors for cells in difference metastasis status when seeded on platforms with different topographies [12]. It is suggested that the topographical structure of the scaffold platforms provided more edges for cell attachment and focal adhesion formation, which favors cell movement [37], [38]. It has been demonstrated that confined microchannels could trigger the modulation of intracellular signalling and morphology changes [39]. Previous study on cell migration speed on flat, 10, 20, and 40 μm wide microchannels showed that

narrow channels enhanced cell moving speed [13], so the 10 μm trenches may also favors the migration of traversed cells in this study.

2) MORE NP460 CELLS SQUEEZED INTO NARROW TRENCHES AFTER TGF-β1 ACTIVATION

As PDMS is a transparent biocompatible material, the position of cells on the platforms under BF microscopy can be observed as shown in Fig. 4 (a). NP460 cells elongated along the grating orientation of the top layer and migrated with a sheet-like structure called lamellipodia as indicated in the SEM in Fig. 4 (a). Some NP460 cells treated with TGF-β1 stayed on the top ridges as the untreated NP460 cells but some exhibited traversing behaviors, i.e. they moved into the 10 μm wide trenches, which were not common to untreated NP460 cells. The number of NP460 cells that migrated into 10 μm wide trenches of the two-layer scaffold platforms during the 15 h of imaging (defined by the percentage of cells that were found in the 10 μm wide trenches continuously for more than 10 h of the entire imaging duration) was tracked as shown in Fig. 4 (b). While the majority of untreated NP460 cells remained on the ridges of the top layer, 21% of the TGF-β1 stimulated NP460 cells squeezed into the 10 μm wide trenches of the scaffold platforms.

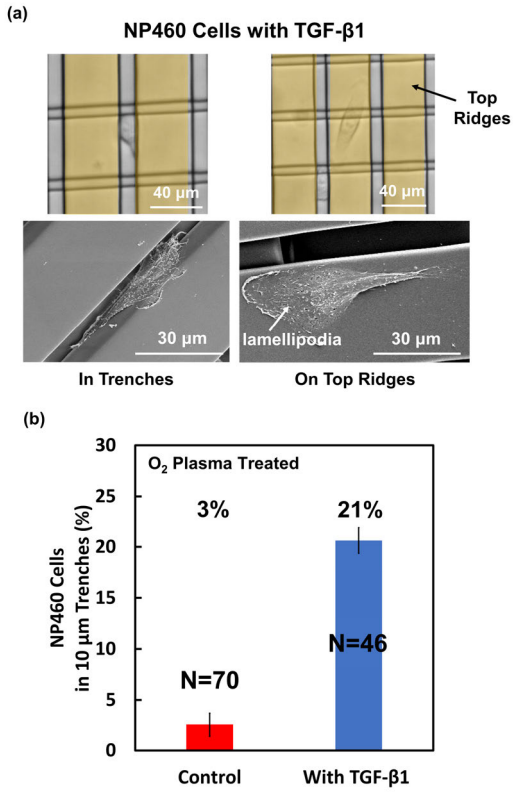

FIGURE 4. (a) Micrographs of NP460 cells with TGF-β1 squeezed into trenches and stayed on ridges of top layer of two-layer scaffold platforms. (b) Percentage of NP460 cells traversed into 10 μm trenches.

These data suggest that untreated NP460 cells preferred to adhere to the 40 μm wide ridges on the top layer as the ridge width more than double the size of the NP460 cells. The 10 μm wide trenches can be regarded as a confined environment that was relatively inaccessible to the cells, preventing them from traversing to the bottom layer. However, the TGF-β1 treated NP460 cells became more invasive with the ability to squeeze into the 10 μm wide trenches which were much narrower than their cell size. As demonstrated previously, TGF-β1 treatment induced rearrangement of vimentin and β-catenin in NP460 cells, which enhanced the cell motility and adhesion [40]–[42]. Previous study also demonstrated that TGF-β1 induced EMT on normal epithelial cells promoted their migration behaviors and invasiveness [43]. In this project, TGF-β1 induced enhancement of cell migration and traversing behaviors of NP460 cells were demonstrated on the designed scaffold platforms, which enabled the likelihood of NP460 cells to reach the less accessible 10 μm wide trenches.

C. SELECTIVELY EXTRACELLULAR MATRIX COATING OF DOUBLE- LAYER SCAFFOLD PLATFORM

The effects of the FN coating on the platforms on NP460 cell migration were investigated. FN is a type of glycoprotein that can be found in ECM, which is important in wound healing and exists in pathological tissue progression. It helps in cell adhesion, growth, movement, and differentiation [44]–[46]. The roles of FN in carcinogenesis and malignant transformation are not fully understood. Some reports suggest that FN can work as a tumor suppressor and restrict the migratory of tumor cells [47]. However, other studies show that the presence of FN elevates the migration, angiogenesis, and invasion [47]–[49]. Many studies introduced FN coating to their designed microsystems to study cell attachment, wound-healing, and chemical responses of cells [27], [50], [51]. In this project, FN was coated onto the double-layer scaffold platforms in two different ways: on top ridges only or fully covered. From Supplementary Fig. S2, immunofluorence was used to characterize the distribution of FN on the platforms after coating. FN fluorescent signal was found on ridges, sidewalls, and trenches from both layers when the platforms were fully covered with FN. On the other hand, FN signal can only be found on the top ridges if FN was coated on top of the platforms.

1) EFFECT OF FIBRONECTIN COATING ON TOP RIDGES ONLY

As shown in Fig. 5 (a) for the two-layer scaffold platforms with FN coating on the top ridges, while untreated NP460 cells migrated randomly with a deviation angle of 38°, NP460 cells after TGF-β1 treatment moved with better alignment to the grating orientation of the top layer with a 54° deviation angle. NP460 cells without TGF-β1 treatment demonstrated similar migration speed as on O_2 plasma-treated scaffold platforms at 0.25 μm/min, but the TGF-β1 treated NP460 cells migrated faster by 0.1 μm/min when seeded on platforms with FN-coated top ridges as shown in Fig. 5 (b). NP460 cells with TGF-β1 treatment

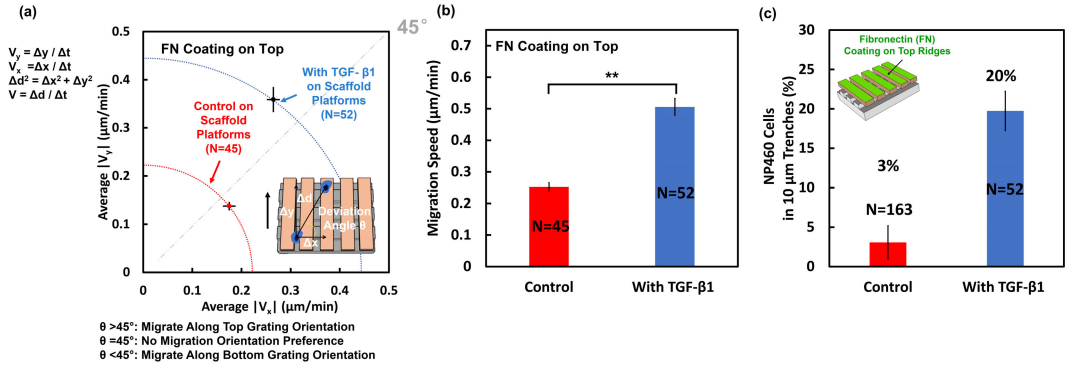

FIGURE 5. NP460 cells with and without TGF-β1 on two-layer scaffold platforms with FN coating on top ridges. (a) NP460 cell migration speed and orientation preference. (b) Migration speed of NP460 cells with and without TGF-β1 (one-way ANOVA test, **p<0.01). (c) Percentage of NP460 cells traversed into 10 μm trenches.

on scaffold platforms with FN coating on top ridges demonstrated significant increase in migration speed compared to untreated NP460 cells (**p<0.01, one-way ANOVA).

The number of NP460 cells with and without TGF-β1 treatment that migrated into the 10 μm wide trenches was monitored under BF microscopy as mentioned previously. As shown in Fig. 5 (c), for scaffold platforms with FN coating on top ridges only, most untreated NP460 cells stayed on 40 μm wide ridges on top layer while 20% of the TGF-β1 treated NP460 cells migrated into the narrow trenches. This result is similar to cell migration on scaffold platforms treated with an O_2 plasma only, as shown in Fig. 4. Most untreated NP460 cells moved on the top layer since only 3% of cells were able to squeeze into the 10 μm wide trenches which were much smaller than their cell size. Some NP460 cells activated by TGF-β1 still traversed into the 10 μm wide trenches, regardless of the FN coating on the top ridges.

2) FIBRONECTIN COATING ENHANCED TRAVERSING BEHAVIOR OF TGF-β1-TREATED CELLS

When the scaffold platforms were fully covered with FN, no untreated NP460 cells migrated into the 10 μm wide trenches as shown in the SEM in Fig. 6 (a). Untreated NP460 cells could only travel on the ridges of the top layer on scaffold platforms treated with O_2 plasma only. Even if the NP460 cells migrated next to the 10 μm wide trenches, they hanged on top of the trenches by attaching to the top ridges on both sides and were not be able to squeeze into the narrow trenches. However, the stimulated NP460 cells on FN coated scaffold platforms were found on the top ridges, moved between the top and bottom layers, and squeezed into the 10 μm wide trenches as shown in Fig. 6 (b). Fewer untreated NP460 cells migrated into the 10 μm wide trenches with FN coating when compared to those without FN coating as only cells squeezed into the trenches for more than 10 h during imaging were included as traversed cells. FN coating in the trenches also enhanced the migration of untreated NP460 cells, allowing them to migrate back to the top ridges easily and move between the ridges and the trenches during imaging, so they were not considered as traversed cells.

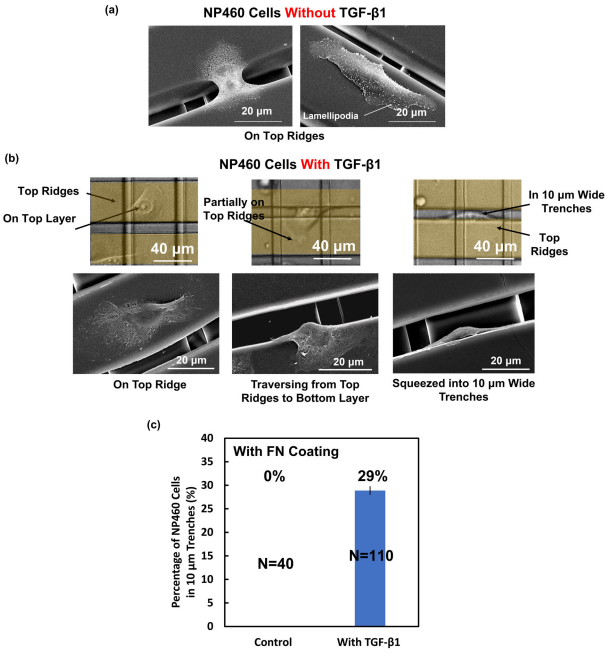

FIGURE 6. Micrographs of NP460 cells (a) without and (b) with TGF-β1 on two-layer scaffold platforms fully covered with FN. (c) Percentage of NP460 cells traversed into 10 μm trenches of scaffold platforms fully covered with FN.

29% of the TGF-β1 treated NP460 cells squeezed into and migrated in the 10 μm wide trenches during the 15 h of time-lapse imaging as demonstrated in Fig. 6 (c). More TGF-β1 treated NP460 cells traversed into the narrow trenches because of the presence of FN coated on the sidewalls of trenches and the bottom layer compared to only 20% with FN was coated only on the top ridges. FN coated on the scaffold platforms promoted the adhesion and migration of NP460 cells. Similar to some wound-healing assays, FN is usually used to stimulate cell adhesion and direct cell migration [46], [52]. These results show that the scaffold platforms fully coated with FN had enlarged the difference of NP460 cells with and without TGF-β1 treatment migration into 10 μm wide trenches when compared with the scaffold

platforms exposed to an O_2 plasma only. Furthermore, the FN coated scaffold platforms could better mimic the extracellular environment, which is full of different biomolecules, and they could be a better representation of cell migration behaviors as an *in vitro* microenvironment study.

Figure 7 (a) shows the migration speed of NP460 cells with and without TGF-β1 treatment on the two-layer scaffold platforms fully coated with FN. Both NP460 cells with and without TGF-β1 treatment became more active and moved faster by 0.2 μm/min when compared to the cells on scaffold platforms treated with an O_2 plasma only. This is consistent with previous findings that show FN promotes cell motility [44]–[46] and induces EMT [53]. Interestingly, on the fully FN-coated platform, the migration speed of TGF-β1 treated NP460 cells was significantly faster than that the ones without TGF-β1 stimulation (**$p<0.01$, one-way ANOVA). Figure 7 (b) shows the migration orientation preference of NP460 cells on FN coated, two-layer scaffold platforms. The deviation angle measured from x-axis for NP460 cells with and without TGF-β1 treatment over the 15 h of imaging period were 63° and 56°, respectively. Therefore, NP460 cells migrated with better alignment to the grating orientation of the top layer on platforms that were fully coated with FN. It is suggested that the NP460 cells became more sensitive to the topographical changes on the platforms with FN coating, perhaps related to the improved cell-surface interaction by enhancing the biocompatibility and hydrophilicity of the PDMS substrate [54].

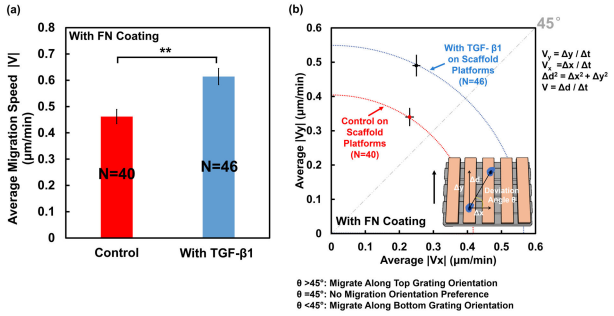

FIGURE 7. (a) Migration speed of NP460 cells on FN coated two-layer scaffold platforms with and without TGF-β1 (one-way ANOVA test, **$p<0.01$). (b) Cell migration speed and orientation preference of NP460 cells on FN coated two-layer scaffold platforms.

Taken together, this study demonstrates that this two-layer scaffold platform can be used to access the changes in EMT on cell invasiveness that is otherwise only detectable by the use of specific biomarkers. Commercially available methods, such as ClearView Chemitaxis Assay, also allows the monitoring of cell migration and invasion for screening application. Laser-etching is used to fabricate the basement membrane with pores for cell penetration. This technique allows rapid prototyping to create structures with different dimensions, but the production time and cost will increase with the hole density or reduced size. In this project, scaffold platforms were fabricated by the imprint technology, which is much faster for production than laser etching. The described assay is constructed with pores on a flat membrane and the change of cell behaviour is observed by quantifying the number of cells passed through the pores only. The traversing behaviour of cells relies on the chemoattractant gradient across the porous membrane, which would change over time and affect the cell migration behavior. The 10 μm wide trenches of our proposed 3D platform acted the same as the pores of the assay but without the need of maintaining stable chemoattractant gradient while the aligned edged from the grating structures also provided physical guidance to the cells. These platforms with topographies provided a more physiologically relevant microenvironment than a flat surface. It also allowed the changes in cell migration speed to be identified, which could not be observed on flat surface according to Fig. 3 (b). As invasiveness was measured by monitoring the traversing behavior of cells, the effectiveness of metastasis-modifying drugs can potentially be determined by low cost BF time-lapse imaging, without the aid of expensive and time-consuming immunofluorescent staining of biomarkers. The use of ECM-coated scaffold platforms in HTS is a promising way to improve the accuracy and cost-effectiveness of *in vitro* drug discovery.

III. MATERIALS AND METHODOLOGY

A. FABRICATION TECHNOLOGY FOR ENGINEERED TWO-LAYER SCAFFOLD PLATFORMS

The fabrication technology for the biomimetic scaffold platforms is shown in Fig. 1. A silicon (Si) stamp with 15 μm deep grating patterns was firstly created by deep reactive ion etching with SPR6112 positive resist as an etch mask patterned on Si using photolithography. The Si stamp was then coated with anti-sticking trichloro (1H, 1H, 2H, 2H-perfluorooctyl) silane (FOTS, 97%, J&K Scientific) at 80 °C for 2 h. The surface energy of the Si stamp with FOTS coating was 17±1 mN/m. Mixture of PDMS prepolymer with curing agent (Dow Corning Sylgard 184 kit) in 10:1 mass ratio was prepared. To fabricate the bottom layer of the scaffold platforms, 2 mm thick PDMS mixture was casted on the Si stamp with 15 μm deep grating patterns and baked at 80 °C for 6 h.

The 15 μm thick top layer of the scaffold platform was created using imprint lithography as shown in Fig. 1 (a). A flat Si was firstly coated with a mixture of 3-methacryloxypropyltrichlorosilane (J&K Scientific) and FOTS in 4:1 (v/v) ratio at 80 °C for 2 h, which resulted in surface energy of 23±3 mN/m. A PDMS layer was then spin-coated on the flat Si at 5700 rpm for 1 min. After imprint under 40 bars at 130 °C for 5 min, the grating structures were transferred from the Si stamp onto the PDMS on the flat Si, which had a higher surface energy. In Fig. 1 (b), the thin PDMS residual layer after the imprint was removed by reactive ion etching with 5 sccm O_2, 20 sccm SF_6, 10 mTorr, and 250 W radio frequency (RF) power for 5 min. To bond the imprinted 15 μm thick top layer with the 2 mm thick bottom layer, both PDMS layers were treated with an O_2 plasma with

20 sccm O_2, 80 mTorr, and 60 W RF power for 1 min, which resulted with a surface energy of 71±3 mN/m. Then the two layers were bonded together at 80 °C for 3 min with the top layer aligned at 90° offset to the bottom layer. After detaching the top layer from the flat Si, the scaffold platforms were created as shown in the micrograph. The scaffold platform was attached to a 35 mm confocal dish and treated with an O_2 plasma with 20 sccm O_2, 80 mTorr, and 60 W RF power for 1 min to increase the hydrophilicity for better cell attachment to the platform.

B. FIBRONECTIN COATING AND IMMUNOFLUORESCENCE STAINING

Other than O_2 plasma surface treatment, the scaffold platforms were also coated with fibronectin (FN, 50 μg/ml in deionized water, Cytoskeleton, Inc.) in some experiments. To ensure the complete coverage of the entire scaffold platform with FN, the platform was treated with an O_2 plasma with 20 sccm O_2, 80 mTorr, and 60 W RF power for 1 min, and FN was added at 18 °C for 1 h under ventilation before seeding cells. The O_2 plasma enhanced the hydrophilicity of the platform with resulted surface energy of 71±3 mN/m.

Contact printing technique as reported in our previous work was used to coat FN only on the ridges of top layer [58]. A 3 mm thick PDMS layer was first casted on a flat Si and baked at 80 °C for 6 h. The cured flat PDMS layer was covered with FN at 18 °C for 2 h under ventilation. After treating the scaffold platform with an O_2 plasma with 20 sccm O_2, 80 mTorr, and 60 W RF power for 1 min, the FN coated PDMS was contacted with the platform for 1 min. Because of the strong surface energy from the O_2 plasma treated scaffold platform, FN from the flat PDMS was transferred onto the top ridges of the scaffold platform.

To stain the FN coated on the two-layer scaffold platforms, they were incubated with primary antibody against FN (1:150, Santa Cruz Biotechnology, Inc.) diluted in phosphate-buffered saline (PBS) at 4 °C overnight. After washing with PBS three times, the samples were kept in the dark with anti-mouse IgG Alexa Fluor 488 (1:500, Merck Millipore) diluted in PBS at room temperature for 2 h. The fluorescent images were then taken using a confocal microscope (SPE, Leica).

C. CELL CULTURE AND TGF-β1 TREATMENT

NP460 (stably expressing LifeAct-fused green fluorescent protein) immortalized cells were used in this project. 1:1 mixture of EpiLife medium (with 1% EpiLife defined growth supplement, Gibco) and defined keratinocyte serum-free medium (with 0.2% defined keratinocyte growth supplement, Gibco) was used to culture NP460 cells added with 1% penicillin/streptomycin (P/S, 10000 U/ml, Gibco). The medium was renewed every two days while the cells were kept in an incubator with 5% CO_2 supply maintained at 37 °C.

NP460 cells were seeded in a 6-well plate with a density of 2 x 10^5 cells per well for 24 h before adding the recombinant human TGF-β1 (PeproTech) at 5 ng/ml for 24 h.

D. IMMUNOFLUORESCENCE OF VIMENTIN AND β-CATENIN

NP460 cells were seeded on coverslips in a 6-well plate at a density of 1 x 10^5 cells/well and incubated overnight at 37 °C with 5% CO_2 supply. TGF-β1 at 1 ng/ml working concentration was added for 24 h. The cells were then rinsed with 1X PBS and kept at room temperature with 4% paraformaldehyde (PFA) for 15 min for fixation. Permeabilization of cells were performed using 0.25% Triton X-100 in PBS at room temperature for 5 min. Blocking buffer with 1% bovine serum albumin in 0.05% Tween-20/PBS (PBST) was used for 30 min under room temperature for the blockage. To investigate the EMT, NP460 cells were incubated with primary antibodies against vimentin (1:200, Cell Signaling) and β-catenin (1:100, Cell Signaling) diluted in the blocking buffer overnight at 4 °C. After washing the cells with PBST three times, the cells were kept in dark at room temperature with anti-rabbit IgG Alexa Fluor 555 conjugate (1:500, Invitrogen) diluted in PBST for 1 h. The cells were then rinsed with PBS and incubated in the dark for 10 min with Hoechst 33342 (Sigma Aldrich) in 1 μg/ml diluted in PBS for nucleus counterstaining. Prolong glass antifade mountant (Thermo Fisher) was used to mount the samples onto glass slides and a confocal microscope was used for fluorescent imaging.

E. TIME-LAPSE BRIGHT-FIELD IMAGING AND DATA ANALYSIS

The two-layer scaffold platform was placed on a 35 mm confocal dish and treated with an O_2 plasma before seeding NP460 cells. The NP460 cells with or without TGF-β1 treatment at a density of 8-10 x 10^4 cells/ml were seeded onto the platforms. After incubating the cells at 37 °C with 5% CO_2 supply for 6 h for the initial attachment, the culturing medium was removed and replaced as reported previously [18] by a mixture of NP460 cell culture medium and CO_2 independent medium (Gibco) with 10% fetal bovine serum, 1% GlutaMAX supplement and 1% P/S in 1:1 (v/v) ratio. An upright microscope (Nikon Eclipse NI-U) with a 20X objective together with a 37 °C incubator without CO_2 supply was used to capture time-lapse images of cells on the two-layer scaffold platforms every 5 min for 15 h.

NIH ImageJ with manual tracking plugin (version 1.50i) was used to analyze the cell migration time-lapse images. The responses of cells were monitored on scaffold platforms with three different surface conditions, namely O_2 plasma treated, FN coated on top ridges, and fully covered with FN. The size of the platform was 2 mm x 2 mm. Each condition was repeated two to three times (within 20 passages) and at least 20 single cells from each run that did not divide or contact with other cells within the 15 h imaging time were included in the analysis. The total number of single cells included from all repeated experiments (N) was labelled in the figures. The fluorescence intensity of vimentin and β-catenin were quantified for more than ten randomly picked cells using NIH ImageJ by recording the region of interest which was defined as the area of a whole cell. One-way ANOVA was used to test

the significant differences while the results are presented as mean ± standard error of the mean.

F. SCANNING ELECTRON MICROSCOPY

After the time-lapse imaging, the cells were rinsed with PBS and fixed by 4% PFA for 15 min. The dehydration process to fix cells involved immersing the sample into deionized water and a series of graded ethanol concentration (30%, 50%, 70%, 80%, 90%, 95% and 100%) while the cells stayed in each ethanol concentration for 5 min. Critical point dryer was used for the dehydration by transitioning the ethanol environment into CO_2. The cells on the scaffold platforms were then coated with gold and imaged by a scanning electron microscope (Hitachi SU5000).

IV. CONCLUSION

In this study, PDMS scaffold platforms consisted of double layers of 15 μm thick grating structures with 40 μm wide ridges and 10 μm wide trenches were designed and fabricated using imprint lithography for screening molecules that induce or inhibit EMT of cells. On the O_2 plasma treated two-layer scaffold platforms, NP460 cells with TGF-β1 treatment migrated faster by 60% than untreated NP460 cells but no migration directionality was observed for both types for cells. Only 2% of the untreated NP460 cells could squeeze into the 10 μm wide trenches while 21% of the TGF-β1 treated NP460 cells were found in the 10 μm wide trenches. When the top ridges of the scaffold platforms were coated with FN, 20% of the TGF-β1 treated NP460 cells traversed into the 10 μm wide trenches and only 3% of the untreated NP460 cells migrated into the trenches. However, when the entire scaffold platforms were covered with FN, all untreated NP460 cells stayed on the top layer while 29% of the TGF-β1 treated NP460 cells traversed from top layer to the bottom layer since the FN in the trenches and bottom layers acted as chemoattractant that enhanced the cell adhesion and migration on the FN coated surfaces.

ACKNOWLEDGMENT

The authors gratefully acknowledge Prof. S. W. Tsao and Prof. C. M. Tsang from the School of Biomedical Science, The University of Hong Kong, for providing the cell line studied in this project. They greatly appreciate the technical support from the staff at the Centre for Biosystems, Neuroscience, and Nanotechnology, the Optoelectronics Laboratory, and the Department of Chemistry.

AUTHOR CONTRIBUTIONS

B.P.L. developed the microfabrication technologies, conducted the experiments, analyzed the results, and wrote the original draft. Y.W.L. reviewed and edited the manuscript. S.W.P. led the project and provided the resources. All authors reviewed the manuscript.

CONFLICT OF INTEREST

There are no conflicts to declare.

REFERENCES

[1] Yang, Wang, Zang, Tang, and Li, "Cell-based assays in high-throughput screening for drug discovery," *Int. J. Biotechnol. Wellness Ind.*, vol. 1, pp. 31–51, Apr. 2012, doi: 10.6000/1927-3037.2012.01.01.02.

[2] G. Du, Q. Fang, and J. M. J. den Toonder, "Microfluidics for cell-based high throughput screening platforms—A review," *Analytica Chim. Acta*, vol. 903, pp. 36–50, Jan. 2016, doi: 10.1016/j.aca.2015.11.023.

[3] N. T. Elliott and F. Yuan, "A review of three-dimensional *in vitro* tissue models for drug discovery and transport studies," *J. Pharmaceutical Sci.*, vol. 100, no. 1, pp. 59–74, Jan. 2011, doi: 10.1002/jps.22257.

[4] Y. K. Kurokawa and S. C. George, "Tissue engineering the cardiac microenvironment: Multicellular microphysiological systems for drug screening," *Adv. Drug Deliv. Rev.*, vol. 96, pp. 225–233, Jan. 2016, doi: 10.1016/j.addr.2015.07.004.

[5] H. F. Lu, M. F. Leong, T. C. Lim, Y. P. Chua, J. K. Lim, C. Du, and A. C. A. Wan, "Engineering a functional three-dimensional human cardiac tissue model for drug toxicity screening," *Biofabrication*, vol. 9, no. 2, May 2017, Art. no. 025011, doi: 10.1088/1758-5090/aa6c3a.

[6] R. Y. Tam, J. Yockell-Lelièvre, L. J. Smith, L. M. Julian, A. E. G. Baker, C. Choey, M. S. Hasim, J. Dimitroulakos, W. L. Stanford, and M. S. Shoichet, "Rationally designed 3D hydrogels model invasive lung diseases enabling high-content drug screening," *Adv. Mater.*, vol. 31, no. 7, Feb. 2019, Art. no. 1806214, doi: 10.1002/adma.201806214.

[7] A. Skardal, M. Devarasetty, S. Forsythe, A. Atala, and S. Soker, "A reductionist metastasis-on-a-chip platform for in vitro tumor progression modeling and drug screening," *Biotechnol. Bioeng.*, vol. 113, no. 9, pp. 2020–2032, Sep. 2016, doi: 10.1002/bit.25950.

[8] B.-J. Jin, S. Lee, and A. S. Verkman, "Hollow micropillar array method for high-capacity drug screening on filter-grown epithelial cells," *Anal. Chem.*, vol. 90, no. 12, pp. 7675–7681, Jun. 2018, doi: 10.1021/acs.analchem.8b01554.

[9] L. Li, Q. Zhou, T. C. Voss, K. L. Quick, and D. V. LaBarbera, "High-throughput imaging: Focusing in on drug discovery in 3D," *Methods*, vol. 96, pp. 97–102, Mar. 2016, doi: 10.1016/j.ymeth.2015.11.013.

[10] S. Wink, "Quantitative high content imaging of cellular adaptive stress response pathways in toxicity for chemical safety assessment," *Chem Res Toxicol*, vol. 27, no. 3, pp. 338–355, Mar. 2014, doi: 10.1021/tx4004038.

[11] Q. Y. Tang, "Control of cell migration direction by inducing cell shape asymmetry with patterned topography," *J. Biomed. Mater. Res. A*, vol. 103, no. 7, pp. 2383–2393, Jul. 2015, doi: 10.1002/jbm.a.35378.

[12] S. F. Zhou, S. Gopalakrishnan, Y. H. Xu, S. K. Y. To, A. S. T. Wong, S. W. Pang, and Y. W. Lam, "Substrates with patterned topography reveal metastasis of human cancer cells," *Biomed. Mater.*, vol. 12, no. 5, Aug. 2017, Art. no. 055001, doi: 10.1088/1748-605X/aa785d.

[13] A. Pathak and S. Kumar, "Independent regulation of tumor cell migration by matrix stiffness and confinement," *Proc. Nat. Acad. Sci. USA*, vol. 109, no. 26, pp. 10334–10339, Jun. 2012, doi: 10.1073/pnas.1118073109.

[14] K. M. Stroka, "Water permeation drives tumor cell migration in confined microenvironments," *Cell*, vol. 157, no. 3, pp. 611–623, Apr. 2014, doi: 10.1016/j.cell.2014.02.052.

[15] M. Wang, B. Cheng, Y. Yang, H. Liu, G. Huang, L. Han, F. Li, and F. Xu, "Microchannel stiffness and confinement jointly induce the mesenchymal-amoeboid transition of cancer cell migration," *Nano Lett.*, vol. 19, no. 9, pp. 5949–5958, Sep. 2019, doi: 10.1021/acs.nanolett.9b01597.

[16] A. W. Lee, W. T. Ng, Y. H. Chan, H. Sze, C. Chan, and T. H. Lam, "The battle against nasopharyngeal cancer," *Radiother Oncol*, vol. 104, no. 3, pp. 272–278, Sep. 2012, doi: 10.1016/j.radonc.2012.08.001.

[17] S. W. Tsao, C. M. Tsang, and K. W. Lo, "Epstein–Barr virus infection and nasopharyngeal carcinoma," *Phil. Trans. Roy. Soc. B, Biol. Sci.*, vol. 372, no. 1732, Oct. 2017, Art. no. 20160270, doi: 10.1098/rstb.2016.0270.

[18] C. M. Tsang, Z. Y. Liu, W. Zhang, C. You, G. E. Jones, S. W. Tsao, and S. W. Pang, "Integration of biochemical and topographic cues for the formation and spatial distribution of invadosomes in nasopharyngeal epithelial cells," *Acta Biomaterialia*, vol. 101, pp. 168–182, Jan. 2020, doi: 10.1016/j.actbio.2019.10.043.

[19] E. Meulmeester and P. Ten Dijke, "The dynamic roles of TGF-beta in cancer," *J Pathol*, vol. 223, no. 2, pp. 205–218, Jan. 2011, doi: 10.1002/path.2785.

[20] Y. Katsuno, S. Lamouille, and R. Derynck, "TGF-β signaling and epithelial–mesenchymal transition in cancer progression," *Current Opinion Oncol.*, vol. 25, no. 1, pp. 76–84, Jan. 2013, doi: 10.1097/CCO.0b013e32835b6371.

[21] B. Li, W. Shen, H. Peng, Y. Li, F. Chen, L. Zheng, J. Xu, and L. Jia, "Fibronectin 1 promotes melanoma proliferation and metastasis by inhibiting apoptosis and regulating EMT," *OncoTargets Therapy*, vol. Volume 12, pp. 3207–3221, May 2019, doi: 10.2147/OTT.S195703.

[22] J. Roche, "The Epithelial-to-Mesenchymal transition in cancer," *Cancers*, vol. 10, no. 2, p. 52, Feb. 2018, doi: 10.3390/cancers10020052.

[23] D. Kloss, "Microcavity array (MCA)-based biosensor chip for functional drug screening of 3D tissue models," *Biosens Bioelectron.*, vol. 23, no. 10, pp. 1473–1480, May 2008, doi: 10.1016/j.bios.2008.01.003.

[24] X. Ma, J. Liu, W. Zhu, M. Tang, N. Lawrence, C. Yu, M. Gou, and S. Chen, "3D bioprinting of functional tissue models for personalized drug screening and *in vitro* disease modeling," *Adv. Drug Del. Rev.*, vol. 132, pp. 235–251, Jul. 2018, doi: 10.1016/j.addr.2018.06.011.

[25] E. Tomecka, K. Zukowski, E. Jastrzebska, M. Chudy, and Z. Brzozka, "Microsystem with micropillar array for three- (gel-embaded) and two-dimensional cardiac cell culture," *Sens. Actuators B, Chem.*, vol. 254, pp. 973–983, Jan. 2018, doi: 10.1016/j.snb.2017.07.186.

[26] B. Jing, Y. Luo, B. Lin, J. Li, Z. A. Wang, and Y. Du, "Establishment and application of a dynamic tumor-vessel microsystem for studying different stages of tumor metastasis and evaluating anti-tumor drugs," *RSC Adv.*, vol. 9, no. 30, pp. 17137–17147, May 2019, doi: 10.1039/c9ra02069a.

[27] J.-H. Lee, K.-L. Ho, and S.-K. Fan, "Liver microsystems *in vitro* for drug response," *J. Biomed. Sci.*, vol. 26, no. 1, p. 88, Oct. 2019, doi: 10.1186/s12929-019-0575-0.

[28] K. Ndyabawe and W. S. Kisaalita, "Engineering microsystems to recapitulate brain physiology on a chip," *Drug Discovery Today*, vol. 24, no. 9, pp. 1725–1730, Sep. 2019, doi: 10.1016/j.drudis.2019.06.008.

[29] A. C. Romano, E. M. Espana, S. H. Yoo, M. T. Budak, J. M. Wolosin, and S. C. Tseng, "Different cell sizes in human limbal and central corneal basal epithelia measured by confocal microscopy and flow cytometry," *Invest. Ophthalmol. Vis. Sci.*, vol. 44, no. 12, pp. 5125–5129, Dec. 2003, doi: 10.1167/iovs.03-0628.

[30] M. Hosokawa, "Size-based isolation of circulating tumor cells in lung cancer patients using a microcavity array system," *PLoS ONE*, vol. 8, no. 6, Jun. 2013, Art. no. e67466, doi: 10.1371/journal.pone.0067466.

[31] L. McInroy and A. Maatta, "Down-regulation of vimentin expression inhibits carcinoma cell migration and adhesion," *Biochem Biophys Res Commun*, vol. 360, no. 1, pp. 14–109, Aug. 17 2007, doi: 10.1016/j.bbrc.2007.06.036.

[32] R. A. Battaglia, S. Delic, H. Herrmann, and N. T. Snider, "Vimentin on the move: New developments in cell migration," *FResearch*, vol. 7, p. 1796, Nov. 2018, doi: 10.12688/f1000research.15967.1.

[33] E. Sanchez-Tillo, O. de Barrios, L. Siles, M. Cuatrecasas, A. Castells, and A. Postigo, "β-catenin/TCF$_4$ complex induces the epithelial-to-mesenchymal transition (EMT)-activator ZEB1 to regulate tumor invasiveness," *Proc. Nat. Acad. Sci. USA*, vol. 108, no. 48, pp. 19204–19209, Nov. 29 2011, doi: 10.1073/pnas.1108977108.

[34] C. Averett, S. Arora, H. Zubair, S. Singh, A. Bhardwaj, and A. P. Singh, "Molecular targets of Honokiol: A promising phytochemical for effective cancer management," *Enzymes*, vol. 36, pp. 93–175, Dec. 2014, doi: 10.1016/B978-0-12-802215-3.00009-4.

[35] C.-M. Yang, S. Ji, Y. Li, L.-Y. Fu, T. Jiang, and F.-D. Meng, "β-catenin promotes cell proliferation, migration, and invasion but induces apoptosis in renal cell carcinoma," *OncoTargets Therapy*, vol. 10, pp. 711–724, Feb. 2017, doi: 10.2147/OTT.S117933.

[36] M. J. Biggs, R. G. Richards, S. McFarlane, C. D. Wilkinson, R. O. Oreffo, and M. J. Dalby, "Adhesion formation of primary human osteoblasts and the functional response of mesenchymal stem cells to 330nm deep microgrooves," *J. Roy. Soc. Interface*, vol. 5, no. 27, pp. 1231–1242, Oct. 2008, doi: 10.1098/rsif.2008.0035.

[37] A. T. Nguyen, S. R. Sathe, and E. K. Yim, "From nano to micro: Topographical scale and its impact on cell adhesion, morphology and contact guidance," *J. Phys. Condens. Matter*, vol. 28, no. 18, May 2016, Art. no. 183001, doi: 10.1088/0953-8984/28/18/183001.

[38] C. D. Paul, W. C. Hung, D. Wirtz, and K. Konstantopoulos, "Engineered models of confined cell migration," *Annu. Rev. Biomed. Eng.*, vol. 18, pp. 80–159, Jul. 2016, doi: 10.1146/annurev-bioeng-071114-040654.

[39] C. Y. Liu, H. H. Lin, M. J. Tang, and Y. K. Wang, "Vimentin contributes to epithelial-mesenchymal transition cancer cell mechanics by mediating cytoskeletal organization and focal adhesion maturation," *Oncotarget*, vol. 6, no. 18, pp. 15966–15983, Jun. 2015, doi: 10.18632/oncotarget.3862.

[40] J. Shankar and I. R. Nabi, "Actin cytoskeleton regulation of epithelial mesenchymal transition in metastatic cancer cells," *PLoS ONE*, vol. 10, no. 3, Mar. 2015, Art. no. e0119954, doi: 10.1371/journal.pone.0119954.

[41] B. Sun, Y. Fang, Z. Li, Z. Chen, and J. Xiang, "Role of cellular cytoskeleton in epithelial-mesenchymal transition process during cancer progression," *Biomed. Rep.*, vol. 3, no. 5, pp. 603–610, Sep. 2015, doi: 10.3892/br.2015.494.

[42] T. H. Wu, Y. W. Chiou, W. T. Chiu, M. J. Tang, C. H. Chen, and M. L. Yeh, "The F-actin and adherence-dependent mechanical differentiation of normal epithelial cells after TGF-beta1-induced EMT (tEMT) using a microplate measurement system," *Biomed Microdevices*, vol. 16, no. 3, pp. 465–478, Jun. 2014, doi: 10.1007/s10544-014-9849-1.

[43] B. Hubbard, J. A. Buczek-Thomas, M. A. Nugent, and M. L. Smith, "Fibronectin fiber extension decreases cell spreading and migration," *J. Cell Physiol.*, vol. 231, no. 8, pp. 1728–1736, Aug. 2016, doi: 10.1002/jcp.25271.

[44] S. Gopal, L. Veracini, D. Grall, C. Butori, S. Schaub, S. Audebert, L. Camoin, E. Baudelet, A. Radwanska, S. Beghelli-de la Forest Divonne, S. M. Violette, P. H. Weinreb, S. Rekima, M. Ilie, A. Sudaka, P. Hofman, and E. Van Obberghen-Schilling, "Fibronectin-guided migration of carcinoma collectives," *Nature Commun.*, vol. 8, no. 1, Jan. 2017, Art. no. 14105, doi: 10.1038/ncomms14105.

[45] A. J. Zollinger and M. L. Smith, "Fibronectin, the extracellular glue," *Matrix Biol.*, vols. 60–61, pp. 27–37, Jul. 2017, doi: 10.1016/j.matbio.2016.07.011.

[46] T.-C. Lin, C.-H. Yang, L.-H. Cheng, W.-T. Chang, Y.-R. Lin, and H.-C. Cheng, "Fibronectin in cancer: Friend or foe," *Cells*, vol. 9, no. 1, p. 27, Dec. 2019, doi: 10.3390/cells9010027.

[47] K. Wang, B. R. Seo, C. Fischbach, and D. Gourdon, "Fibronectin mechanobiology regulates tumorigenesis," *Cellular Mol. Bioeng.*, vol. 9, no. 1, pp. 1–11, Mar. 2016, doi: 10.1007/s12195-015-0417-4.

[48] Y.-C. Ou, J.-R. Li, J.-D. Wang, C.-Y. Chang, C.-C. Wu, W.-Y. Chen, Y.-H. Kuan, S.-L. Liao, H.-C. Lu, and C.-J. Chen, "Fibronectin promotes cell growth and migration in human renal cell carcinoma cells," *Int. J. Mol. Sci.*, vol. 20, no. 11, p. 2792, Jun. 2019, doi: 10.3390/ijms20112792.

[49] E. Jastrzebska, A. Zuchowska, S. Flis, P. Sokolowska, M. Bulka, A. Dybko, and Z. Brzozka, "Biological characterization of the modified poly(dimethylsiloxane) surfaces based on cell attachment and toxicity assays," *Biomicrofluidics*, vol. 12, no. 4, Jul. 2018, Art. no. 044105, doi: 10.1063/1.5035176.

[50] S. M. Weiz, M. Medina-Sánchez, and O. G. Schmidt, "Microsystems for single-cell analysis," *Adv. Biosystems*, vol. 2, no. 2, Feb. 2018, Art. no. 1700193, doi: 10.1002/adbi.201700193.

[51] C.-T. Hsiao, H.-W. Cheng, C.-M. Huang, H.-R. Li, M.-H. Ou, J.-R. Huang, K.-H. Khoo, H. W. Yu, Y.-Q. Chen, Y.-K. Wang, A. Chiou, and J.-C. Kuo, "Fibronectin in cell adhesion and migration via N-glycosylation," *Oncotarget*, vol. 8, no. 41, pp. 70653–70668, Sep. 2017, doi: 10.18632/oncotarget.19969.

[52] C.-L. Li, D. Yang, X. Cao, F. Wang, D.-Y. Hong, J. Wang, X.-C. Shen, and Y. Chen, "Fibronectin induces epithelial-mesenchymal transition in human breast cancer MCF-7 cells via activation of calpain," *Oncol. Lett.*, vol. 13, no. 5, pp. 3889–3895, May 2017, doi: 10.3892/ol.2017.5896.

[53] P. Formentín, Ú. Catalán, L. Pol, S. Fernández-Castillejo, R. Solá, and L. F. Marsal, "Collagen and fibronectin surface modification of nanoporous anodic alumina and macroporous silicon for endothelial cell cultures," *J. Biol. Eng.*, vol. 12, no. 1, p. 21, Dec. 2018, doi: 10.1186/s13036-018-0111-x.

[54] J. Hui and S. W. Pang, "Cell migration on microposts with surface coating and confinement," *Biosci. Rep.*, vol. 39, no. 2, p. 51, Feb. 2019, doi: 10.1042/BSR20181596.

BOWIE P. LAM received the B.S. degree in electronic engineering from the City University of Hong Kong, Hong Kong, in 2018.

From 2018 to 2020, she was a Research Assistant with the Centre for Biosystems, Neuroscience, and Nanotechnology, City University of Hong Kong. Her research interests include micro- and nano-fabrication for bio MEMS, implantable devices, and biosensors.

YUN WAH LAM was born in Hong Kong, in 1968. He received the Ph.D. degree in biochemistry from The University of Hong Kong, in 1997.

After his Ph.D., he received his postdoctoral training at the Wellcome Trust Biocentre, Dundee, Scotland. In 2007, he joined the City University of Hong Kong as an Assistant Professor, where he became an Associate Professor in 2010. He is the author of over 100 research articles and three book chapters and is the holder of two patents. He works with a multidisciplinary research network that consists of biochemists, chemists, materials scientists, and medical doctors, to tackle a variety of biological projects, ranging from biomedical engineering, environmental sciences to regenerative medicine.

Dr. Lam is a Council Member of the Hong Kong Biochemistry and Molecular Biology Society, the Founder and the Organiser of the Hong Kong Chapter of Leonardo Art Science Evening Rendezvous (LASER), and the 2019 Resident at SymbioticA, a centre for biological art in The University of Western Australia. He won the Second Prize of Roche's ''Imagining the Future'' Competition in 2006.

STELLA W. PANG (Fellow, IEEE) received the B.Sc. degree from Brown University, Providence, RI, USA, in 1977, and the M.Sc. and Ph.D. degrees from Princeton University, Princeton, NJ, USA, in 1978 and 1981, respectively.

From 1981 to 1989, she was with the Lincoln Laboratory, Massachusetts Institute of Technology, Cambridge, MA, USA. From 1990 to 2011, she was a Professor of Electrical Engineering and Computer Science and the Associate Dean of the Graduate Education and International Programs with the College of Engineering, University of Michigan at Ann Arbor, Ann Arbor, MI, USA, from 2002 to 2007. She is currently a Chair Professor and the Head of the Department of Electrical Engineering, City University of Hong Kong, Hong Kong, where she is also the Director of the Center for Biosystems, Neuroscience, and Nanotechnology. She has over 400 technical articles, book chapters, and invited presentations and is an editor and an author of 16 books, journals, and conference proceedings. She has nine patents granted in nanotechnology and microsystems. She has taught 32 short courses on microfabrication and nanoimprint technology for microelectronic manufacturing and microelectromechanical systems. Her research interests include nanofabrication technology for biomedical, microelectromechanical, microelectronic, and optical devices.

Dr. Pang is a Fellow of The Electrochemical Society (ECS), the American Vacuum Society (AVS), and The Hong Kong Institution of Engineers (HKIE). She has served as a Conference Organizer for AVS, ECS, the IEEE Electronic Materials Conference, the International Symposium on Electron, Ion, and Photon Beam Technology and Nanofabrication, the Material Research Society, and SPIE.